JOURNAL OF NANO- AND ELECTRONIC PHYSICS
Vol. **7** No 3, 03011(5pp) (2015)

ЖУРНАЛ НАНО- ТА ЕЛЕКТРОННОЇ ФІЗИКИ
Том **7** № 3, 03011(5cc) (2015)

A First Principles Study of Chalcopyrite Mn-doped $AlGaP_2$ Compounds

Byung-Sub Kang*, Kie-Moon Song†

Nanotechnology Research Center, Nano Science & Mechanical Engineering,
Konkuk University, 380-701 Chungju, South Korea

(Received 25 May 2015; published online 20 October 2015)

We studied the electronic and magnetic properties for the Mn-doped chalcopyrite $AlGaP_2$ semiconductor by using the first-principles calculations. The Mn-doped $AlGaP_2$ yields strong half-metallic ground states. The ferromagnetic state is the most energetically favorable one. The states of host Al, Ga, or P atoms at the Fermi level are mainly a P-3*p* character, which mediates a strong interaction between the Mn-3*d* and P-3*p* states. The ferromagnetic ordering of dopant Mn with high magnetic moment is originated from the P(3*p*)-Mn(3*d*)-P(3*p*) hybridization, which is attributed by the partially filled P-3*p* bands. The high magnetic moment of Mn by P vacancy is produced by 4.2 μ_B/Mn.

Keywords: Chalcopyrite $AlGaP_2$ semiconductor, Band-structure, Ferromagnetism, First-principles.

PACS numbers: 71.15.Ap, 71.55.Gs

1. INTRODUCTION

Diluted magnetic semiconductor (DMS) materials have become a great interest because the charge from the *s* and *p* electrons of the nonmagnetic semiconductor, and the spin from the magnetic dopant can be used in spintronics devices. A recent strategy to achieve further control over the spin degree of freedom is based on dilute ferromagnetic semiconductors, prepared by substituting magnetic ions such as V, Cr, Mn, Fe, Co, and Ni into non-magnetic semiconductor hosts. Ferromagnetism has been reported in various semiconductor groups including II-VI [1, 2] and III-V [3-5] such as GaN, ZnO, and so on. However, to date, the low solubility of magnetic ions in non-magnetic semiconductor hosts has limited the opportunities. When ferromagnetic metals are used as spin injectors, the polarization in the semiconductor tends to be quickly lost via spin-flip scattering. It is one of the primary challenges to create the ferromagnetic semiconductors due to the difficulty in the spin-injection into the semiconductors to form DMS at room temperature or above room temperature.

Accordingly, the conventional DMS had a low solubility of magnetic ions in host semiconductors. An approach in enhancing the solubility is to make a monolayer super lattice [6], and another is to find a new pure ferromagnetic semiconductor. Recently, a newly synthesized a $MnGeP_2$ compound has been reported as a semiconductor, whose crystal structure is chalcopyrite. It has been reported that $MnGeP_2$ exhibits ferromagnetism with $T_c = 320$ K and a magnetic moment per Mn at 5 K of 2.58 μ_B, and an indirect energy gap of 0.24 eV. Moreover, it has been reported that the Mn-doped chalcopyrite such as $ZnSnAs_2$ [7] and $ZnGeP_2$ [8] shows ferromagnetic ordering at 320 and 312 K, respectively. Chalcopyrite, which are 'genealogically' related to the more familiar tetrahedrally-coordinated zinc-blende materials, are a class of semiconductors recognized as promising materials for nonlinear optical applications.

In the present works, we studied by using first-principle calculations for the electronic and magnetic properties of $(Al_{1-y}Mn_y)GaP_2$ and $Al(Ga_{1-y}Mn_y)P_2$ with $y = 0.03125$, 0.0625, 0.09375, and 0.125 DMS. In Mn-doped $AlGaP_2$ chalcopyrite semiconductor, we observed ferromagnetic ordering. The ferromagnetic Mn-doped $AlGaP_2$ chalcopyrite is the most energetically favorable one. Total energy calculations predicted that the ternary compound $AlGaP_2$ is indirect semiconductor with band gaps of 0.75 eV. The spin polarized $Al(GaMn)P_2$ state (Al-rich system) is more stable than that of $(AlMn)GaP_2$ state (Ga-rich system) with the magnetic moment of 3.8 μ_B/Mn. The Mn-doped $AlGaP_2$ yields strong half-metallic ground states. We noted that this chalcopyrite and related materials can replace the Mn-doped III-V systems and open the way to room temperature spintronic devices.

2. COMPUTATIONAL METHODOLOGY

The first-principles simulations were performed using the full-potential linear muffin-tin orbital (FP-LMTO) method based on the framework of the density-functional theory [9]. The muffin-tin radii of Mn (or Al, Ga) and P were chosen to be 2.4 and 1.9 a.u., respectively. The final set of energies was computed with the plane-wave cutoff energy of 596.63 eV. The convergence tests of the total energy with respect to the plane-wave energy cutoff and *k*-point sampling had been carefully examined. Brillouin zone integrations were performed with the special k-point method over a gamma-centered $4 \times 4 \times 4$ mesh. It is corresponding to 64 *k*-points. It insured that the total energies and the magnetic moments were converged on a better 10 meV/cell and 0.01 μ_B/atom scale, respectively. The exchange-correlation energy of the electrons was described in the generalized gradient approximation (GGA) as proposed in Perdew-Burke-Ernzerhof function [10].

The LMTO basis set and charge density were expanded in terms of the spherical harmonics up to $l = 6$

* kangbs@kku.ac.kr
† kmsong@kku.ac.kr

inside each muffin-tin sphere. The LMTO basis functions in the valence energy region were chosen as 4*s* and 3*d* for Mn, and 4*s*, 4*p*, and 3*d* for Ga. The basis function of Mn (or Al) for the 4*s* (or 3*s*), 4*p* (or 3*p*), and 3*d* is generated with cut-off energy of 159.12 eV, 232.56 eV, and 340.0 eV, respectively. The valence electrons were not assumed to have the spin-orbital coupling but had generated the self-consistent supercell potential by considering the scalar relativistic effects. The atomic potentials were approximated by spherically symmetric potential. However, the full charge-density, including all non-spherical terms, was evaluated in Fourier series in the interstitial region on the FPLMTO method.

3. RESULTS AND DISCUSSION

For the AlP, GaP, and pure $AlGaP_2$ systems, we considered the atomic relaxations for the positions of the structures. However, the distortions of near host atoms by substituting Mn dopant in the $AlGaP_2$ bulk were neglected. The III-III-V_2 alloy crystallizes in a form of $AlGaP_2$ chalcopyrite structure, which is related to a familiar tetrahedrally-coordinated zinc-blende crystal structure. The calculated lattice parameters are $a = 5.726$ Å and $c = 11.452$ Å for GaP; $a = 5.648$ Å and $c = 11.296$ Å for AlP. For $AlGaP_2$, they are $a = 5.685$ Å, $c = 11.222$ Å, and $c/a = 1.974$. In the calculations for the GaP and AlP systems, we performed a minimization of the total energy for the supercell volume when keeping the constant c/a ratio (= 2.0). For the $AlGaP_2$ system, we considered the structural relaxation for each of a and c-axis. The calculated parameters for GaP and AlP can be compared with that of the zinc-blende structure. The experimental values are $a = 5.451$ Å and 5.450 Å for GaP [11, 12] and AlP [11], respectively. The tetrahedral chalcopyrite structure was displayed in the Fig. 1. These structures for GaP, $AlGaP_2$, and AlP exhibit the semiconducting character with energy gaps of 1.679 eV, 1.241 eV, and 0.276 eV, respectively. It shows a downward bowing of the lattice parameter as increases Al concentration in the $Al_xGa_{1-x}P_2$ system ($x = 0.0$, 0.25, 0.75, and 1.0). While for the calculated band-gap, it increases from 0.276 eV to 1.679 eV. These results of the band-gap are smaller than the experimental values [13]. In general, the value of band-gap calculated using the GGA is less than half of the value obtained in the experiment. Maybe it can be obtained the result that the calculated value in the LDA + U [14] is slightly larger than that in the GGA.

Using the optimally calculated lattice parameters, we carried out the calculations for total energies in the (Al, Mn)GaP_2 system (in the case of Ga-rich system) with replacing Al atoms by dopant Mn, in the Al(Ga, Mn)P_2 with replacing Ga atom by Mn, and in AlGa(P, Mn)$_2$ of P substitution by Mn. The (Al, Mn)GaP_2 is the case of Ga-rich system, the Al(Ga, Mn)P_2 is the case of Al-rich system. It can be seen that the Al(Ga, Mn)P_2 is the lowest energetically favorable system from the Table 1. However, its difference in their energies is small in comparison with these systems. The defect energy and the substitution energy with a vacancy of Al, Ga, or P were defined as, respectively.

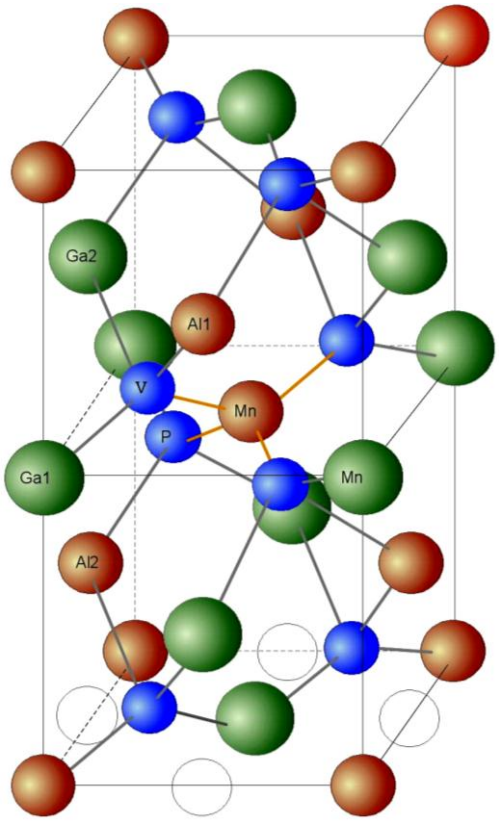

Fig. 1 – Crystal structure of chalcopyrite $AlGaP_2$. Open-circles represent interstitial sites in a layer. V denotes the defect by P vacancy

Table 1 – Substitution energies and magnetic moments for the dopant-site of Mn in $AlGaP_2$. Total energy difference between FM and AFM (antiferromagnetic) states for Ga-rich (Al, Mn)GaP_2 and Al-rich Al(Ga, Mn)P_2, and AlGa(P, Mn)$_2$ ($E_{total}(FM) - E_{total}(AFM)$, in eV). Mn_1 and $Mn_{1.5}$ correspond to the concentration of 6.25 % and 9.375 %, respectively.

Systems	Substitution Energy (meV)	Magnetic moment in FM/AFM state (μ_B/Mn)	Total Energy Difference (meV)
$(Al_{3.0}Mn_{1.0})GaP_2$	– 282.2	3.84 /– 3.84	– 99.7
$(Al_{2.5}Mn_{1.5})GaP_2$	–	3.80 /– 3.78	– 352.6
$(Al_{2.0}Mn_{2.0})GaP_2$	–	3.72 /– 3.72	– 464.5
$Al(Ga_{3.0}Mn_{1.0})P_2$	– 346.5	3.79	–
$AlGa(P_{3.5}Mn_{0.5})_2$	– 270.7	2.70	–

$$E_d = E\left(AlGaP_2; V\left(Al/Ga/P\right)\right) - E\left(AlGaP_2\right) + \\ + \bar{n}_1\mu_{Al} \pm \bar{n}_2\mu_{Ga} \pm \bar{n}_3\mu_P \quad (1)$$

$$E_{d,sub} = E\left(AlGaP_2; Mn, V\left(Al/Ga/P\right)\right) - E\left(AlGaP_2\right) \pm \\ \pm \bar{n}_1\mu_{Al} \pm \bar{n}_2\mu_{Ga} \pm \bar{n}_3\mu_P - \bar{n}_4\mu_{Mn} \quad (2)$$

where $E(AlGaP_2; V(Al/Ga/P))$ is the total energies of the pure $AlGaP_2$ with the vacancy of 3.125 % Al, Ga, or P concentration. $E(AlGaP_2; Mn, V(Al/Ga/P))$ and $E(AlGaP_2)$ are the total energies of Mn-doped $AlGaP_2$ with a vacancy (of 3.125 % concentration of Al, Ga, or

P) and the pure $E(AlGaP_2)$ reference structure, respectively. μ_{Mn}, μ_{Al}, μ_{Ga}, and μ_P are the atom chemical potentials of Mn, Al, Ga, and P, while the integers n_1, n_2, n_3, and n_4 are the number of doped Mn atoms, and substituted Al, Ga, and P atoms, respectively. The chemical potentials depend on the experimental conditions under which the material is grown. In order to determine these quantities, we invoke the relationship $\mu_{Al} + \mu_{Ga} + 2\mu_P = \mu_{AlGaP2}$, assuming these species are in thermal equilibrium with $AlGaP_2$. The atomic chemical potential for Mn is assumed to be determined by equilibrium with bulk MnP, which is the FM phase with a Neel temperature of 291 K [13].

$\mu_{Al} = E(AlP(bulk)) - E(P(bulk))$ and
$\mu_{Ga} = E(GaP(bulk)) - E(P(bulk))$. Under Al-rich conditions, $\mu_{Mn} = E(MnP(bulk)) - E(AlP(bulk)) + E(Al(bulk))$ and $\mu_P = E(AlP(bulk)) - E(Al(bulk))$; and under Ga-rich conditions,
$\mu_{Mn} = E(MnP(bulk)) - E(GaP(bulk)) + E(Ga(bulk))$ and $\mu_P = E(GaP(bulk)) - E(Ga(bulk))$.

Table 2 – Defect energies (E_d, eV) for undoped $AlGaP_2$ and substitution energies ($E_{d,sub}$, eV) for Mn-doped $AlGaP_2$ with the vacancy of 3.125 % Al, Ga, or P concentration. Δ denotes the total energy difference between the substitution and defect energies. The parentheses are the magnetic moment of Mn within the FM state

Defect elements	E_d (eV)	$E_{d,sub}$ (eV)	Δ (meV)
Al	8.432	8.706 (3.5 μ_B/Mn)	+ 0.274
Ga	7.736	7.895 (3.4 μ_B/Mn)	+ 0.159
P	9.294	8.989 (4.2 μ_B/Mn)	– 0.305

The Mn dopant orders ferromagnetically in $AlGaP_2$. The FM state is more energetically favorable than the nonmagnetic or antiferromagnetic (AFM) state. The difference in total energy between the FM and AFM states is – 34.72 meV in the Mn concentration of 6.25 %. In the case of $Al(Ga_3Mn_1)P_2$, the nearest neighboring four surrounding P atoms formed the MnP_4 tetrahedron are aligned positively with magnetic moments of 0.05 μ_B per P atom. While for the nearest neighboring Al or Ga atoms, it is aligned negatively with magnetic moment of ~ – 0.02 μ_B per Al or Ga atom. The substituted Mn atom has the magnetic moment with a localized magnetic moment of 3.84 μ_B/Mn. In the case of P vacancy in $AlGaP_2$, the total energy difference between the substitution energy by Mn and defect energy is the lowest. The Mn magnetic moment for Mn-doped $AlGaP_2$ with a vacancy is increased by 4.2μ_B/Mn more than that without a vacancy. These results were listed in the Table 2.

Fig. 2 shows the band structures for the pure $AlGaP_2$ and the systems with Al, Ga, or P vacancy of 3.125 %. The band shift in the case of P vacancy is larger than other systems. This because that it shows a strong interaction in their P-3*p* states, or between P-3*p* state and Mn-3*d* states at the Fermi level (E_F). It can

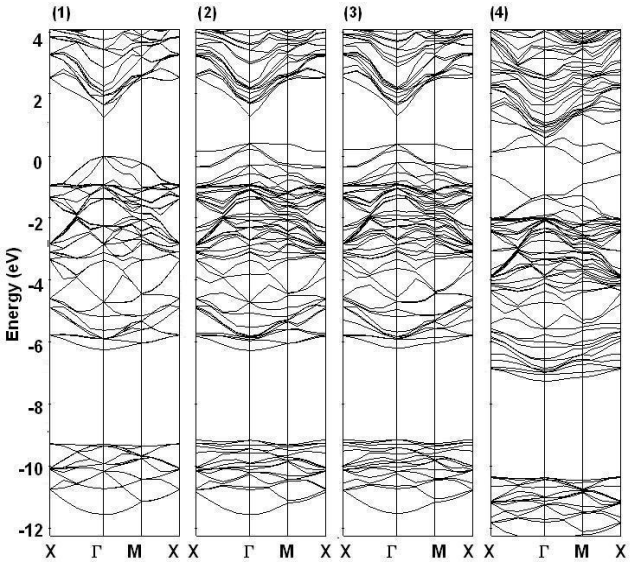

Fig. 2 – Band structures for perfect $AlGaP_2$ (1) and $AlGaP_2$ with Al vacancy (2), with Ga vacancy (3), or with P vacancy (4). The concentration of defect is 3.125 %. The Fermi level is set to zero

be seen in reduced states just at the E_F. Fig. 3 shows the density of states (DOS) for Al-rich $Al(GaMn)P_2$ of 6.25 % Mn and for Ga-rich $(AlMn)GaP_2$ with P vacancy of 3.125 % concentration. We could observe the perturbation of the valence band by dopant Mn in the host $AlGaP_2$ bands. The band of majority state on the E_F occupies Al-3*p* and Ga-4*p*, and P-3*p* electrons mainly. These majority *p* states make a result of strong hybridization between the P-3*p* (or Al-3*p*, or Ga-4*p*) and Mn-3*d* (t_2, d_{xy}) bands, or Mn-3d (e, d_{x2-y2}) bands. The partially filled Mn *e*-band lies on the E_F (mainly majority states), while the t_2-band falls into the valence band by E_F – 2.5 eV. Especially, a strong interaction between Mn-3*d* and P-3*p* occurs due to the carrier accumulation between the Mn and neighboring P atoms just on the E_F. Hence the partially filled p band (mainly P-3*p* electrons) and a defect P bands contribute to the ferromagnetism with high magnetic moment. These configurations provide us with clues to elucidate the mechanism of the carrier (holes)-mediated ferromagnetism in Mn-doped $AlGaP_2$.

The substituted system of Al or Ga by Mn atom shows the half-metallic character due to downward shift of the host Al, Ga, and P minority bands. The Mn-P bond in $Al(GaMn)P_2$ is largely covalent because a strong interaction between the Mn-3*d* and P-3*p* states.

The direct Mn 3*d*-3*d* correlation between Mn atoms may be small because the variance of magnetic moment with respect to the Mn concentration is not change nearly. Thus the ferromagnetism of Mn dopant maybe implies a direct exchange mechanism by the P site. When it exhibits the substitution of Al or Ga by Mn, the Mn and P atoms forms the P-Mn-P bond. The strong hybridization between P-3*p* and Mn-3*d* states is reduced in the system of P vacancy; a high magnetic moment of Mn is maintained.

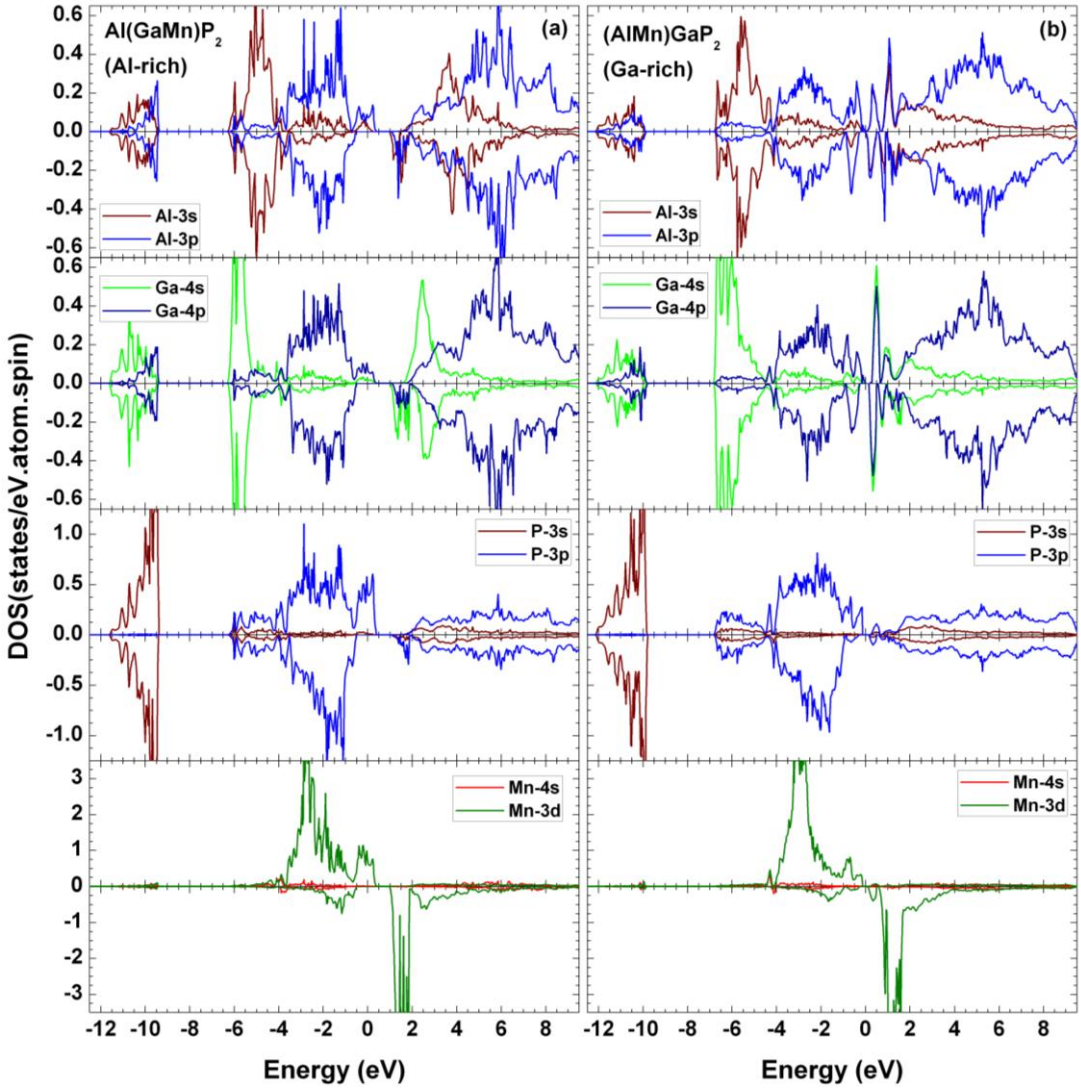

Fig. 3 – (a) DOS for Al, Ga, P, and Mn sites of Al-rich $Al(GaMn)P_2$ (6.25 % Mn) in the FM state. (b) DOS for Al, Ga, P, and Mn sites of $(AlMn)GaP_2$ (3.125 % Mn) with a vacancy of P in the FM state. The Fermi level is set to zero

4. CONCLUDING REMARKS

We had investigated the electronic structure and magnetic properties of Mn-doped $AlGaP_2$ chalcopyrite semiconductor by using the first-principles calculations. The $AlGaP_2$ chalcopyrite compound is a *p*-type semiconductor with a band gap of 1.23 eV. For Mn-doped $AlGaP_2$, the FM state is the most energetically favorable than the other states. We had observed that this system exhibits the FM and half-metallic ground state. In the defect system of P vacancy, it shows weak half-metallic ground state. It illustrates the stability of FM state with respect to the Mn-doping concentration. The ferromagnetism of dopant Mn is produced by the partially filled P-3*p* bands. The high magnetic moment of Mn is maintained by the hybridized P(3*p*)-Mn(3*d*)-P(3*p*) interaction. It is necessary to study more in the DMS limit. We expect it to be an application of useful DMS in the spintronics.

AKNOWLEDGEMENTS

This work was supported by Konkuk University (Dept. of Nano science and Mechanical engineering) in 2015.

REFERENCES

1. T. Fukumura, Zhengwu Jin, A. Ohtomo, H. Koinuma, M. Kawasaki, *Appl. Phys. Lett.* **75**, 3366 (1999).
2. K. Sato, H. Katayama-Yoshida, *phys. status solidi (b)* **229**, 673 (2002).
3. Priya Mahadevan, Alex Zunger, *Phys. Rev. B* **69**, 115211 (2004).
4. X.Y. Cui, J.E. Medvedeva, B. Delley, A.J. Freeman, C. Stampfl, *Phys. Rev. B* **75**, 155205 (2007).
5. S.J. Pearton, C.R. Abernathy, D.P. Norton, A.F. Hebard, Y.D. Park, L.A. Boatner, J.D. Budai, *Mater. Sci. Eng. R* **40**, 137 (2003).
6. J. Choi, S. Choi, S.C. Hong, S. Cho, M.H. Sohn, Y. Park, K.W. Lee, H.Y. Park, J.H. Song, J.B. Ketterson, *J. Korean Phys. Soc.* **47**, S497 (2005).
7. S. Choi, G.-B. Cha, S.C. Hong, S. Cho, Y. Kim, J.B. Ketterson, S.-Y. Jeong, G.-C. Yi, *Solid State Commun.* **122**, 165 (2002).

8. Sunglae Cho, Sungyoul Choi, Gi-beom Cha, Soon Cheol Hong, Yunki Kim, Yu-Jun Zhao, Arthur J. Freeman, John B. Ketterson, B.J. Kim, Y.C. Kim, Byung-Chun Choi, *Phys. Rev. Lett.* **88**, 257203 (2002).
9. S.Y. Savrasov, *Phys. Rev. B* **54**, 16470 (1996).
10. J.P. Perdew, K. Burke, M. Ernzerhof, *Phys. Rev. Lett.* **77**, 3865 (1996).
11. C. Kittel, *Introduction to Solid State Physics. Seventh ed.* (John Wiley & Sons: 1996).
12. Nadir Bouarissa, *Mater. Chem. Phys.* **124**, 336 (2010).
13. S.J. Pearton, C.R. Abernathy, D.P. Norton, A.F. Hebard, Y.D. Park, L.A. Boatner, J.D. Budai, *Mater. Sci. Eng. R* **40**, 137 (2003).
14. J.H. Park, S.K. Kwon, B.I. Min, *Physica B* **281-282**, 703 (2000).